Random Set Based Road mapping using Radar Measurements

Christian Lundquist, Lars Danielsson and Fredrik Gustafsson

Linköping University Post Print

N.B.: When citing this work, cite the original article.

Original Publication:

Christian Lundquist, Lars Danielsson and Fredrik Gustafsson, Random Set Based Road mapping using Radar Measurements, 2010, Proceedings of the European Signal Processing Conference, 219-223.

Copyright: Eurasip

Postprint available at: Linköping University Electronic Press http://urn.kb.se/resolve?urn=urn:nbn:se:liu:diva-62849

RANDOM SET BASED ROAD MAPPING USING RADAR MEASUREMENTS

Christian Lundquist[†], Lars Danielsson[‡], and Fredrik Gustafsson[†]

† Department of Electrical Engineering, Division of Automatic Control, Linköping University, SE-581 83 Linköping, Sweden, e-mail: {lundquist, fredrik}@isy.liu.se.

‡ Volvo Car Corporation, Active Safety Electronics, SE-405 31 Göteborg, Sweden, e-mail: ldanie25@volvocars.com

ABSTRACT

This work is concerned with the problem of multi-sensor multi-target tracking of stationary road side objects, i.e. guard rails and parked vehicles, in the context of automotive active safety systems. Advanced active safety applications, such as collision avoidance by steering, rely on obtaining a detailed map of the surrounding infrastructure to accurately assess the situation. Here, this map consists of the position of objects, represented by a random finite set (RFS) of multi-target states and we propose to describe the map as the spatial stationary object intensity. This intensity is the first order moment of a multi-target RFS representing the position of stationary objects and it is calculated using a Gaussian mixture probability hypothesis density (GM-PHD) filter.

1. INTRODUCTION

For an advanced automotive safety application it is important to keep track on stationary object along the road to be able to detect dangerous situations and decide on appropriate actions. The system may warn the driver or intervene by braking or steering to avoid collisions or mitigate its consequences. Information about the current traffic situation is typically obtained from on board radar sensors, as they are robust against different whether conditions and offer accurate measurements of range, angle and range rate to objects.

There exist many algorithms to track or describe stationary objects along the road, see e.g., [1]. Occupancy grid mapping [5] was primarily developed to be used with laser scanners to generate consistent maps. This method was very popular at the DARPA urban challenge, see the special issues [2]. However, it is unadapted for radar sensors and the resulting map may be imprecise as shown in [15].

Road edge and obstacle detection has been tackled using raw radar images, see e.g., [8, 12, 16, 19]. There have been several approaches making use of reflections from the road edges, such as guard rails and reflection posts, to compute information about the free space, see e.g. [10, 11, 21] for some examples using laser scanners. Radar reflections were used to track the road edges as extended targets in [13]. This methods is promising but a drawback is the large data association problem, which arises since it is hard to create a general model for the various types of objects.

The development of finite-set statistics (FISST) by Mahler, see e.g., [6, 17], provides a way to extend the single-sensor single-target Bayes statistics to multi-sensor multi-target Bayes statistics. Mahler developed an algorithm for multi-sensor multi-target tracking, based on FISST, called the Probability Hypothesis Density (PHD) filter, which is a full tracking algorithm in the sense that it both include filtering and data association, see e.g., [18].

Radar reports from stationary objects can be handled within a multi-target framework. In contrast to a single-target system, where uncertainty is characterized by modeling the state and the measurement as random vectors, uncertainty in a multi-target system can be characterized by modeling the multi-target state and multi-sensor measurement as RFS. The PHD filter propagates the posterior intensity, a first order statistical moment of the posterior multi-target state, instead of propagating the posterior density in time.

A Gaussian mixture approximation of the PHD was proposed by Vo and Ma [22]. The mixture is represented by a sum of weighted Gaussian components and in particular the mean and covariance of those components are propagated by the Kalman filter [9]. The GM-PHD filter implementation is used in this contribution since it is computational more efficient and noise is assumed Gaussian for the system at hand.

In this work we propose to use the PHD filter framework to calculate the spatial intensity of stationary radar reflectors. The resulting spatial intensity can be viewed as a general map over where there are large concentrations of stationary radar reflectors, i.e. the position of guard rails and parked vehicles. In contrast to traditional multi-target tracking algorithms, we are not interested in keeping a separate track for each radar reflector with a separate unique identifier. Instead, we have the freedom to find a more efficient representation of the information in the radar observations, e.g., by merging closely spaced object.

This contribution is outlined as follows. Beginning with a problem formulation in Section 2, which includes a description of the FISST, the system model and the automotive radar sensors. The PHD filter recursion for the road mapping example is described in Section 3. The resulting posterior intensity can be used as a map describing the surroundings of the vehicle as shown in Section 4. The conclusions are in Section 5.

2. PROBLEM FORMULATION

The aim of this paper is to position stationary radar reflectors, i.e. reflection points on road side objects, such as, guard rails or lampposts, using noisy radar measurements. The ultimate goal being to construct a map over the surrounding infrastructure.

The radar measurements are obtained from N_s radar sensors mounted on the ego vehicle with the measurement spaces $\mathscr{Z}^{(1)},\ldots,\mathscr{Z}^{(N_s)}$. Each sensor $j=1,\ldots,N_s$ collects a random finite set (RFS) $\mathbf{Z}_k^{(j)}$ of individual observations $m=1,\ldots,N_{z,k}$ of range $r^{(m)}$, range rate $\dot{r}^{(m)}$ and azimuth angle $\delta^{(m)}$ to strong radar reflectors according to

$$\left\{\mathbf{z}_{k}^{(m)} = \begin{bmatrix} r^{(m)} & \dot{r}^{(m)} & \delta^{(m)} \end{bmatrix}_{k}^{T} \right\}_{m=1}^{N_{z,k}} \in \mathbf{Z}_{k}, \tag{1}$$

for discrete time instants k = 1, ..., K. All sensors collect together a RFS of observations according to

$$\mathbf{Z}_k = \mathbf{Z}_{\iota}^{(1)} \cup \dots \cup \mathbf{Z}_{\iota}^{(N_s)}. \tag{2}$$

Hence, the single observation spaces can be bundled together into one measurement space, so that any observation must be some finite subset \mathbf{Z}_k of \mathscr{Z} . Put in other words, the multi observations set \mathbf{Z}_k consists of all measurements collected from all targets by all sensors at time step k. The measurement history RFS is denoted $\mathbf{Z}_{1:k}$, and contains the set of all measurements from time 1 to time k.

For the given application measurements from a prototype passenger car equipped with three radars ($N_s = 3$) are used. More specifically, the ego vehicle is equipped with one standard ACC

forward looking 77 GHz mechanically scanned FMCW radar and two medium distance 24 GHz radar mounted at the corners of the vehicle, see Figure 1. Hence, this constitutes a multi-sensor system, measuring at different ranges and in different directions, but with an overlap of observation spaces. Put in other words, the intersection as well as the complement of the single observation spaces $\mathscr{Z}^{(1)}, \ldots, \mathscr{Z}^{(3)}$ are non empty. A coordinate frame E is attached to the moving ego vehicle and its position, orientation and velocity relative the world coordinate frame W is tracked in a sensor fusion framework, but fore the sake of simplicity, assumed to be known in this work.

The sought positions of radar reflectors are represented by their Cartesian position in the world coordinate frame W and stored in the point reflector state vector

$$\mathbf{x}_{k}^{(i)} = \begin{bmatrix} \mathbf{x}^{(i)} & \mathbf{y}^{(i)} \end{bmatrix}^{T}. \tag{3}$$

The stationary reflectors along the road are tracked as a RFS of point reflector given by

$$\mathbf{X}_k = \left\{ \mathbf{x}_k^{(1)}, \dots, \mathbf{x}_k^{(N_{x,k})} \right\},\tag{4}$$

where $N_{x,k}$ is the number of targets at time k.

The state space model of the stationary objects is given by

$$\mathbf{x}_{k+1} = F\mathbf{x}_k + \mathbf{w}_k, \qquad \mathbf{w}_k \sim \mathcal{N}(0, Q), \qquad (5a)$$

$$\mathbf{z}_k = h(\mathbf{x}_k) + \mathbf{e}_k, \qquad \mathbf{e}_k \sim \mathcal{N}(0, R) \qquad (5b)$$

$$\mathbf{z}_k = h(\mathbf{x}_k) + \mathbf{e}_k, \qquad \mathbf{e}_k \sim \mathcal{N}(0, R)$$
 (5b)

where F is the identity matrix, since the objects are not moving. The nonlinear measurement model $h(\mathbf{x}_k)$ describes how a measurement (1) i.e., the range r and the azimuth angle δ relates to the state vector \mathbf{x}_k (3). The Doppler of an object \dot{r} is also measured and is primarily used in the gating to determine if the object is stationary or moving. The nonlinear sensor model is given by

$$h(\mathbf{x}_{k}^{(i)}) = \begin{bmatrix} \sqrt{\left(\mathbf{x}^{(i)} - \mathbf{x}_{E_{s}^{(m)}W}^{W}\right)^{2} + \left(\mathbf{y}^{(i)} - \mathbf{y}_{E_{s}^{(m)}W}^{W}\right)^{2}} \\ -v\cos\left(\arctan\frac{\mathbf{y}^{(i)}}{\mathbf{x}^{(i)}} - \psi_{E_{s}^{(m)}}\right) \\ \arctan\frac{\mathbf{y}^{(i)}}{\mathbf{x}^{(i)}} - \psi_{E_{s}^{(m)}} \end{bmatrix}, \quad (6)$$

where $\boldsymbol{d}_{E_{s}^{(m)}W}^{W} = \begin{bmatrix} \mathbf{x}_{E_{s}^{(m)}W}^{W} & \mathbf{y}_{E_{s}^{(m)}W}^{W} \end{bmatrix}^{T}$ is the position and $\psi_{E_{s}^{(m)}}$ the orientation of the radar sensor $m=1,\ldots,N_{s}$ in the world coordinate frame W.

The first order moment of the RFS X_k is called the intensity or the Probability Hypothesis Density (PHD) and it is denoted v_k . One

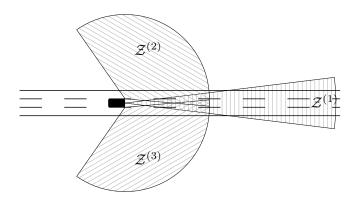


Figure 1: The observation spaces of the front looking radar is denoted $\mathscr{Z}^{(1)}$ and the observation spaces of the side radars are $\mathscr{Z}^{(2)}$ and $\mathcal{Z}^{(3)}$.

important property of the multi-target posterior PHD is that the integral of the PHD over any given volume of the state space yields the expected number of targets present in that volume. However, in our case the interpretation is slightly different. Here, an object, such as guard rails, are likely to be made up of multiple strong radar reflectors. For this reason, the integral over the PHD is not the number of targets, but rather the number of strong radar reflectors and the PHD represent the concentration of these in our two dimensional state space.

Let $v_{k|k}$ and $v_{k+1|k}$ denote the posterior and predicted intensity, respectively. In the present work it is assumed that the intensities of the RFSs are Gaussian mixtures. The posterior intensity at time k is written on the form

$$v_{k|k}(\mathbf{x}) = \sum_{i=1}^{J_{k|k}} w_{k|k}^{(j)} \mathcal{N}\left(\mathbf{x}; m_{k|k}^{(j)}, P_{k|k}^{(j)}\right). \tag{7}$$

In the next section it is described how the intensity is estimated in the PHD-filter.

3. GM-PHD FILTER RECURSION

The GM-PHD filter recursion is well described in e.g. [22] and only briefly summarized here together with additional details for the road mapping example. The PHD recursion given by (8) in Section 3.1 and (17) in Section 3.2 below, constitutes the PHD filter. The merging of Gaussian components is described in Section 3.3.

3.1 Time Evolution

The time evolution of the intensity is given by

$$v_{k+1|k}(\mathbf{x}) = v_{S,k+1|k}(\mathbf{x}) + v_{B,k+1|k}(\mathbf{x}) + \gamma_{k+1}(\mathbf{x})$$
 (8)

where $v_{S,k+1|k}(\mathbf{x})$ is the predicted intensity of the RFS of previous states, $v_{\beta,k+1|k}(\mathbf{x})$ is the intensity of the RFS spawned from a target at time k+1 based on the previous states and $\gamma_{k+1}(\mathbf{x})$ is the intensity of the birth RFS at time k+1. The elements in the sum are described below.

3.1.1 Prediction

The prediction for the existing targets is given by

$$v_{S,k+1|k}(\mathbf{x}) = p_{S,k+1} \sum_{j=1}^{J_{k|k}} w_{k+1|k}^{(j)} \mathcal{N}\left(\mathbf{x}; m_{k+1|k}^{(j)}, P_{k+1|k}^{(j)}\right), \quad (9)$$

where $p_{S,k+1}$ is the probability of survival. The Gaussian components $\mathcal{N}(m_{k+1|k}^{(j)}, P_{k+1|k}^{(j)})$ are derived using the linear process model (5a) and the time update step of the Kalman according to

$$m_{k+1|k}^{(j)} = F m_{k|k}^{(j)},$$
 (10a)

$$P_{k+1|k}^{(j)} = F P_{k|k}^{(j)} F^{\mathsf{T}} + Q_k. \tag{10b}$$

3.1.2 Birth

The intensity of the birth RFS is assumed to be a Gaussian mixture

$$\gamma_{k+1}(\mathbf{x}) = \sum_{i=1}^{J_{\gamma,k+1}} w_{\gamma,k+1}^{(j)} \, \mathcal{N}\left(\mathbf{x}; m_{\gamma,k+1}^{(j)}, P_{\gamma,k+1}^{(j)}\right), \tag{11}$$

where $w_{\gamma,k+1}^{(j)}$, $m_{\gamma,k+1}^{(j)}$ and $P_{\gamma,k+1}^{(j)}$ for $j=1,\ldots,J_{\gamma,k+1}$, are model parameters that determine the shape of the birth intensity. The birth RFS is modeled as a Poisson RFS, i.e. the cardinality is Poisson distributed, i.e. $J_{\gamma,k+1} \sim \text{Pois}(\lambda)$, and the components $\mathcal{N}(m_{\gamma,k+1}^{(j)}, P_{\gamma,k+1}^{(j)})$ are uniformly distributed over the state space.

The intensity of the spawn RFS is a Gaussian mixture of the form

$$v_{\beta,k+1|k}(\mathbf{x}) = \sum_{j=1}^{J_{\beta,k+1}} w_{\beta,k+1|k}^{(j)} \, \mathcal{N}\left(\mathbf{x}; m_{\beta,k+1|k}^{(j)}, P_{\beta,k+1|k}^{(j)}\right), \quad (12)$$

where $w_{\beta,k+1|k}^{(j)}$, $m_{\beta,k+1|k}^{(j)}$ and $P_{\beta,k+1|k}^{(j)}$ for $j=1,\ldots,J_{\beta,k+1}$, are model parameters that determine the shape of the spawn intensity. The Gaussian mixture components $\mathscr{N}(m_{\beta,k+1|k}^{(j)},P_{\beta,k+1|k}^{(j)})$ are derived using a model based process, which takes the existing Gaussian components $\mathscr{N}(m_{k|k},P_{k|k})$ at time step k as input.

It is assumed that new stationary objects are most likely to be born at the road edges, and a simplified version of the model presented in [14] is utilized to estimate the road edges and create the spawn intensity.

It is common to model a road in the vehicles Cartesian coordinate frame using a third order polynomial, see e.g., [3,4]. We model the road edges in the same manner according to

$$y = a_0 + a_1 x + a_2 x^2 + a_3 x^3, \tag{13}$$

where the x and y-coordinates are expressed in the vehicle's coordinate frame E. The parameters a_0,\ldots,a_3 are estimated using the Gaussian components $\mathcal{N}(m_{k|k},P_{k|k})$, from the time step k. The components are clustered depending on if they belong to the left or right side of the road, and the mean values m are used to solve for the parameters in a least squares curve fitting problem. To simplify the problem, in particular when there are only a few components on one side of the road, it is assumed that the left and right edges of the road are approximately parallel and only differ by the lateral distances a_0 .

A number $J_{\beta,k+1}/2$ of x^E -coordinates, denoted $\left\{x_j^E\right\}_{j=1}^{J_{\beta,k+1}}$, are chosen in the range from 0 to the maximum range of the radar sensor. The corresponding y^E -coordinates $\left\{y_j^E\right\}_{j=1}^{J_{\beta,k+1}/2}$ and $\left\{y_j^E\right\}_{j=J_{\beta,k+1}/2+1}^{J_{\beta,k+1}}$ are derived by using the road border model (13) and the estimated parameters a_0,\ldots,a_3 . The coordinates form the mean values of the position of the Gaussian components on the road edges according to

$$m_{\beta,k+1}^{E,(j)} = \begin{bmatrix} \mathsf{x}_j^E & \mathsf{y}_j^E \end{bmatrix}^{\mathsf{T}}.\tag{14a}$$

The covariance of the Gaussian components is given by the diagonal matrix

$$P_{\beta,k+1}^{E,(j)} = \begin{bmatrix} \left(\sigma_{\mathsf{x}}^{E}\right)^{2} & 0\\ 0 & \left(\sigma_{\mathsf{y}}^{E}(\mathsf{x}_{j}^{E})\right)^{2} \end{bmatrix},\tag{14b}$$

where it is assumed that the variance of the y-coordinate increases with the x-distance, i.e., $\sigma_y^E(\mathbf{x}_j^E)$ depends on \mathbf{x}_j^E .

So far the derivations are accomplished in the ego vehicles coordinate frame E, but since the state variables (4) are expressed in the world frame W, the components of the Gaussian mixture are transformed into the world coordinate frame according to

$$m_{B k+1}^{(j)} = R^{WE} m_{B k+1}^{E,(j)} + \boldsymbol{d}_{EW}^{W}$$
 (15a)

$$P_{\beta,k+1}^{(j)} = R^{WE} P_{\beta,k+1}^{E,(j)} \left(R^{WE} \right)^{\mathrm{T}}.$$
 (15b)

to be used in (12). The planar rotation matrix is given by

$$R^{WE} = \begin{bmatrix} \cos \psi_E & -\sin \psi_E \\ \sin \psi_E & \cos \psi_E \end{bmatrix}, \tag{16}$$

where ψ_E is the angle of rotation from W to E. This angle is referred to as the yaw angle of the vehicle. The position of the vehicle in the world frame W is given by the displacement vector \mathbf{d}_{WW}^{E} .

world frame W is given by the displacement vector \mathbf{d}_{EW}^W . The weight $w_{\beta,k+1}^{(j)}$ represents the expected number of new targets originating from $m_{\beta,k+1}^{(j)}$.

3.2 Measurement Update

The measurement update is given by a sum of intensities according to

$$v_{k|k}(\mathbf{x}) = (1 - p_{D,k})v_{k|k-1} + \sum_{\mathbf{z} \in \mathbf{Z}_k} v_{D,k}(\mathbf{x}|\mathbf{z}). \tag{17}$$

where the probability of detection is adjusted according to

$$p_{D,k}(\mathbf{x}) = \begin{cases} p_{D,k} & \eta_{k|k-1}^{(i)} \in \mathcal{Z}, \\ 0 & \eta_{k|k-1}^{(i)} \notin \mathcal{Z}. \end{cases}$$
(18)

Gaussian components which are outside the sensor's field of view i.e., the measurement space \mathcal{Z} , are not updated. The updated intensity $v_{D,k}(\mathbf{x}|\mathbf{z})$ is given by

$$v_{D,k}(\mathbf{x}|\mathbf{Z}_k) = \sum_{j=1}^{J_{k|k-1}} \sum_{\mathbf{z}_k \in \mathcal{G}_j} w_k^{(j)}(\mathbf{z}_k) \mathcal{N}\left(\mathbf{x}; m_{k|k}^{(j)}(\mathbf{z}_k), P_{k|k}^{(j)}\right), \quad (19)$$

where the cardinality $J_{k|k-1} = J_{k-1|k-1} + J_{\beta,k} + J_{\gamma,k}$. The Gaussian components $\mathcal{N}(m_{k|k}^{(j)}(\mathbf{z}_k), P_{k|k}^{(j)})$ are derived by using the non-linear measurement equation (5b), the measurement update step of the unscented Kalman filter and the information from each new measurements \mathbf{z}_k according to

$$m_{k|k}^{(j)}(\mathbf{z}_k) = m_{k|k-1}^{(j)} + K_k^{(j)} \left(\mathbf{z}_k - \eta_{k|k-1}^{(j)}\right),$$
 (20a)

$$P_{k|k}^{(j)} = P_{k|k-1}^{(j)} - K^{(j)} S_{k|k-1}^{(j)} \left(K^{(j)}\right)^T, \tag{20b}$$

$$K^{(j)} = G_{k|k-1}^{(j)} \left(S_{k|k-1}^{(j)} \right)^{-1},$$
 (20c)

where $S_{k|k-1}^{(j)} \approx \operatorname{Cov}\left(h(\mathbf{x}_k^{(j)})\big|\mathbf{Z}_{k-1}\right)$ and $G_{k|k-1}^{(j)} \approx \operatorname{Cov}\left(\mathbf{x}_k^{(j)}, h(\mathbf{x}_k^{(j)})\big|\mathbf{Z}_{k-1}\right)$, are defined in (22). The gate \mathscr{G}_j is given by

$$\mathscr{G}_{j} = \left\{ \mathbf{z}_{k} \middle| \left(\mathbf{z}_{k} - \boldsymbol{\eta}_{k|k-1}^{(j)} \right)^{T} \left(S_{k|k-1}^{(j)} \right)^{-1} \left(\mathbf{z}_{k} - \boldsymbol{\eta}_{k|k-1}^{(j)} \right) < \delta_{\mathscr{G}} \right\}, \tag{21}$$

for the gate threshold $\delta_{\mathscr{G}}$.

The unscented transform is used to propagate the state variables through the measurement equation, see e.g., [7]. A set of L sigma points and weights, denoted by $\left\{\chi_k^{(\ell)}, u^{(\ell)}\right\}_{\ell=0}^L$ are generated using the method described in [7]. The sigma points are transformed to the measurement space using (6) to obtain the propagated sigma point $\hat{\mathbf{z}}_{k|k-1}^{(\ell)}$ and the first and second order moments of the measurement density is approximated as

$$\eta_{k|k-1}^{(j)} = \sum_{\ell=0}^{L} u^{(\ell)} \hat{\mathbf{z}}_{k|k-1}^{(\ell)}, \tag{22a}$$

$$S_{k|k-1}^{(j)} = \sum_{\ell=0}^{L} u^{(\ell)} \left(\hat{\mathbf{z}}_{k|k-1}^{(\ell)} - \boldsymbol{\eta}_{k|k-1}^{(j)} \right) \left(\hat{\mathbf{z}}_{k|k-1}^{(\ell)} - \boldsymbol{\eta}_{k|k-1}^{(j)} \right)^{T} + R_{k},$$
(22b)

$$G_{k|k-1}^{(j)} = \sum_{\ell=0}^{L} u^{(\ell)} \left(\chi_{k|k-1}^{(\ell)} - m_{k|k-1}^{(j)} \right) \left(\hat{\mathbf{z}}_{k|k-1}^{(\ell)} - \eta_{k|k-1}^{(j)} \right)^{T}. \quad (22c)$$

Furthermore, the weights are updated according to

$$w_k^{(j)}(\mathbf{z}_k) = \frac{p_{D,k} w_{k|k-1}^{(j)} q_k^{(j)}(\mathbf{z}_k)}{\kappa + p_{D,k} \sum_{\ell=1}^{J_{k|k-1}} w_{k|k-1}^{(\ell)} q_k^{(\ell)}(\mathbf{z}_k)},$$
 (23a)

$$q^{(j)}(\mathbf{z}_k) = \mathcal{N}\left(\mathbf{z}_k; \eta_{k|k-1}^{(j)}, S_{k|k-1}^{(j)}\right), \tag{23b}$$

where $\eta_{k|k-1}^{(j)}$ is the predicted measurement and $S_{k|k-1}^{(j)}$ is the innovation covariance. The clutter intensity of the clutter RFS at time k is denoted κ_k .

3.3 Pruning and Merging

The PHD filter suffers from the computational problem that the number of Gaussian components J representing the Gaussian mixture increases as time progresses. To ensure that the complexity of the algorithm is under control, Gaussians with low weights are eliminated trough pruning and Gaussians with similar means are combined through merging. However, the loss of information must be as small as possible in these stages.

The clustering algorithm, proposed by Salmond [20], merges Gaussian components in groups. A cluster center (centroid) is chosen as the component with the largest weight and the algorithm then merges all surrounding components to the centroid. This process is repeated with the remaining components until all have been clustered. The clustering algorithm is used in the original Gaussian mixture PHD filter [22].

4. EXPERIMENTS AND RESULTS

The experiments were conducted with a prototype passenger car, equipped with the radar sensor configuration as shown in Figure 1. Only radar reflections from moving objects are used to update the estimates in this work, hence, the moving objects are not presented here. No reference data of the road borders exist, so one example of the resulting estimated bird's eye view of a freeway traffic scenario in Figure 2b-2c, can only be compared with the corresponding driver's view in Figure 2a. The intensity map $v_{k|k}$ in Figure 2b indicates the probability of occupancy. The map may be used by other automotive safety functions, for instance path planning which aims at minimizing the cumulative PHD along the path. A low intensity indicates a low probability to hit an object. The Gaussian mixture map, in Figure 2c, shows the single Gaussian components $\left\{m_k^{(i)}, P_k^{(i)}\right\}$ illustrated by their mean (black stars) and covariance ellipses, after merge and prune are accomplished. Note that the weights are included in Figure 2b but not in Figure 2c. Figure 2c also shows the radar detections illustrated by red marks. The stars are measurements collected by the front looking radar, the diamonds are from the left radar and the triangles are from the right radar.

The past and future path of the ego vehicle is shown by black dots in the figure and can be used as a good reference of the road edges being correctly estimated. The illustrated road is estimated from image data from the camera, and can also be used as a reference. From the camera view in Figure 2a it can be seen that the road seems to bend slightly to the right. The Gaussians and the intensity, which are based on radar data from the guardrails, have picked up the right bend quite well. The range (field of view) of the radar is approximately 200 m.

5. CONCLUSION

In this work it is shown how stationary objects, measured by standard automotive radar sensors, can be used with a PHD filter to obtain an intensity map of the area surrounding the vehicle. This intensity map describes the density of stationary objects, such as guardrails and lampposts, and may be used by other active safety functions to derive drivable trajectories with low probability of occupancy.

In future work, we plan on investigating a more accurate method to cluster the Gaussian components and model the road edges for the spawning intensity. We also plan to analyze the effects of pruning and merging based on prior knowledge of the road model

REFERENCES

- S. S. Blackman and R. Popoli. *Design and Analysis of Modern Tracking Systems*. Artech House, Inc., Norwood, MA, USA, 1999
- [2] M. Buehler, K. Iagnemma, and S. Singh, editors. Special Issue on the 2007 DARPA Urban Challenge, Part I-III, volume 25 (8-10). *Journal of Field Robotics*, 2008.
- [3] E. D. Dickmanns. *Dynamic Vision for Perception and Control of Motion*. Springer, London, UK, 2007.
- [4] E. D. Dickmanns and A. Zapp. A curvature-based scheme for improving road vehicle guidance by computer vision. In *Pro*ceedings of the SPIE Conference on Mobile Robots, volume 727, pages 161–198, Cambridge, MA, USA, 1986.
- [5] A. Elfes. Sonar-based real-world mapping and navigation. IEEE Journal of Robotics and Automation, 3(3):249–265, June 1987.
- [6] I. R. Goodman, R. P. S. Mahler, and H. T. Nguyen. *Mathematics of data fusion*. Kluwer Academic, Dordrecht, 1997.
- [7] S. J. Julier and J. K. Uhlmann. Unscented filtering and nonlinear estimation. *Proceedings of the IEEE*, 92(3):401–422, March 2004.
- [8] K. Kaliyaperumal, S. Lakshmanan, and K. Kluge. An algorithm for detecting roads and obstacles in radar images. *IEEE Transactions on Vehicular Technology*, 50(1):170–182, January 2001.
- [9] R. E. Kalman. A new approach to linear filtering and prediction problems. *Transactions of the ASME, Journal of Basic Engineering*, 82:35–45, 1960.
- [10] A. Kirchner and C. Ameling. Integrated obstacle and road tracking using a laser scanner. In *Proceedings of the IEEE Intelligent Vehicles Symposium*, pages 675–681, Dearborn, MI, USA, October 2000.
- [11] A. Kirchner and T. Heinrich. Model based detection of road boundaries with a laser scanner. In *Proceedings of the IEEE Intelligent Vehicles Symposium*, pages 93–98, Stuttgart, Germany, 1998.
- [12] S. Lakshmanan, K. Kaliyaperumal, and K. Kluge. Lexluther: an algorithm for detecting roads and obstacles in radar images. In *Proceedings of the IEEE Conference on Intelligent Transportation Systems*, pages 415–420, Boston, MA, USA, November 1997.
- [13] C. Lundquist, U. Orguner, and T. B. Schön. Tracking stationary extended objects for road mapping using radar measurements. In *Proceedings of the IEEE Intelligent Vehicles Symposium*, pages 405–410, Xi'an, China, June 2009.
- [14] C. Lundquist and T. B. Schön. Estimation of the free space in front of a moving vehicle. In *Proceedings of the SAE World Congress*, SAE paper 2009-01-1288, Detroit, MI, USA, April 2009.
- [15] C. Lundquist, T. B. Schön, and U. Orguner. Estimation of the free space in front of a moving vehicle. Technical Report LiTH-ISY-R-2892, Department of Electrical Engineering, Linköping University, SE-581 83 Linköping, Sweden, April 2009.
- [16] B. Ma, S. Lakshmanan, and A.O. Hero. Simultaneous detection of lane and pavement boundaries using model-based multisensor fusion. *IEEE Transactions on Intelligent Transportation Systems*, 1(3):135–147, September 2000.

- [17] R. P. S. Mahler. Proceedings of the International Conference on Information Fusion. Artech House, Boston, 2007.
- [18] R.P.S. Mahler. Multitarget Bayes filtering via first-order multitarget moments. *IEEE Transactions on Aerospace and Electronic Systems*, 39(4):1152–1178, October 2003.
- [19] M. Nikolova and A Hero. Segmentation of a road from a vehicle-mounted radar and accuracy of the estimation. In *Pro*ceedings of the IEEE Intelligent Vehicles Symposium, pages 284–289, Dearborn, MI, USA, October 2000.
- [20] David J. Salmond. Mixture reduction algorithms for target tracking in clutter. Signal and Data Processing of Small Targets, 1305(1):434–445, 1990.
- [21] J. Sparbert, K. Dietmayer, and D. Streller. Lane detection and street type classification using laser range images. In Proceedings of the IEEE Conference on Intelligent Transportation Systems, pages 454–459, Oakland, CA, USA, August 2001.
- [22] Ba-Ngu Vo and Wing-Kin Ma. The Gaussian mixture probability hypothesis density filter. *IEEE Transactions on Signal Processing*, 54(11):4091–4104, Nov. 2006.



(a) Camera view

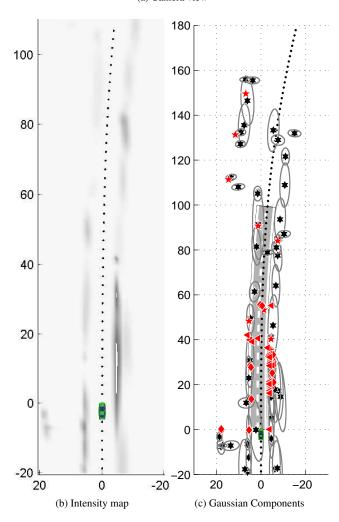


Figure 2: The image in Figure (a) shows the driver's view. The intensity map $v_{k|k}$ is shown in Figure (b). The Gaussian mixture (mean and covariance ellipse) as well as the measurements from the radars are shown in Figure (c). The red stars are obtained by the front radar ($\mathbf{Z} \in \mathscr{Z}^{(1)}$), the diamonds by the left radar ($\mathbf{Z} \in \mathscr{Z}^{(2)}$) and the triangles are by the right radar ($\mathbf{Z} \in \mathscr{Z}^{(3)}$).